Autonomous control of inverter-interfaced Distributed Generation units for harmonic current filtering and resonance damping in an islanded microgrid

Wang, Xiongfei; Blaabjerg, Frede; Chen, Zhe

Published in:
Proceedings of the IEEE Energy Conversion Congress and Exposition 2012

DOI (link to publication from Publisher):
10.1109/ECCE.2012.6342821

Publication date:
2012

Document Version
Early version, also known as pre-print

Autonomous Control of Inverter-Interfaced Distributed Generation Units for Harmonic Current Filtering and Resonance Damping in an Islanded Microgrid

Xiongfei Wang, Frede Blaabjerg, Zhe Chen
Department of Energy Technology
Aalborg University, Aalborg, Denmark
xwa@et.aau.dk, fbl@et.aau.dk, zch@et.aau.dk

***Abstract*—Harmonic current filtering and resonance damping have become important concerns on the control of an islanded microgrids. To address these challenges, this paper proposes a control method of inverter-interfaced Distributed Generation (DG) units, which can autonomously share harmonic currents and resonance damping burdens. The approach employs a load compensator based on the decomposition of output current, in addition to the outer droop-based power controller, as well as inner voltage and current controllers. The load compensator consists of a virtual fundamental impedance loop for enhanced sharing of reactive power, and a variable harmonic impedance loop which allows to counteract harmonic voltage drops across the grid-side inductance of the DG inverter, and to damp the harmonic resonance propagation throughout a distribution feeder. Experiments on a three-phase microgrid are performed to validate the performance of the proposed control scheme.**

I. INTRODUCTION

The microgrid paradigm is emerging as an attractive way to future smart distribution grids, thanks to its capability to operate in both grid-connected and islanded modes [1]. The dynamic islanding operations bring more flexibility on the integration of Distributed Generation (DG) units, and also provide a more reliable electricity service [2]. On the other hand, during the islanded operations, the microgrid usually becomes much weaker and more sensitive to power quality disturbances [3]. Thus, the harmonic distortion tends to be more apparent in an islanded microgrid. Furthermore, since the use of *LCL*-filters is gaining a wide acceptance in grid-connected converters, the aggregated shunt capacitance for a number of *LCL*-filters may lead to harmonic resonance with the line inductance, and the consequent harmonic voltage amplification on a distribution feeder [4]. Hence, stringent demands are being imposed on the ancillary services of inverter-interfaced DG units, such as the mitigation of circulating harmonic current in multiple DG units, harmonic voltage reduction and harmonic resonance damping [5].

A number of research efforts have been made to address the aforementioned challenges [6]-[14]. In [6], the idea of Resistive-Active Power Filter (R-APF) is implemented based on a high-bandwidth current controller, where DG inverters are controlled to behave as resistors at harmonic frequencies, such that harmonic resonances and voltage distortions can be damped. To autonomously share harmonic currents, a droop relationship between the distorted power of a DG inverter and the controlled harmonic resistance is built [7]. However, it has been shown that only the output voltage of a DG unit is regulated in this method, whereas the voltage at the Point of Connection (PoC) tend to be undamped in the presence of grid-side inductance [8]. Another popular scheme is based on the virtual output impedance concept [9]-[12], where a load current feedforward loop is introduced together with a high-bandwidth output voltage controller. Thus, either the virtual inductance or the virtual resistance can be synthesized at the harmonic frequencies. It is essentially a frequency-dependent voltage droop with the output harmonic currents [12]. As a consequence, the additional harmonic voltage distortions are inevitably increased, and even become more severe when a large virtual inductance is needed to attenuate the differences among the grid-side inductances of DG units. To alleviate the adverse effect of the grid-side inductance, a PoC voltage feedforward control scheme is developed recently [13]. With a positive gain G in the PoC voltage feedforward loop, the harmonic impedance seen from the PoC of a DG inverter can be scaled down by $1/(1+G)$. Nevertheless, the performance of this scheme is limited on the harmonic resonance damping due to the absence of additional harmonic resistance.

Considering the adverse effect of the grid-side inductance and the demand of harmonic resonance damping, a Variable Harmonic Impedance (VHI) concept was developed in [14], which comprises positive resistance and negative inductance at the dominant harmonic frequencies. In this paper, the VHI concept is extended for an islanded microgrid with multiple DG inverters, and an autonomous control method of the DG inverters is proposed. The approach is based on a multiloop control scheme, where a load compensator that comprises the

978-1-4673-0803-8/12/$31.00 ©2012 IEEE

Virtual Fundamental Impedance (VFI) and the VHI loops is developed in addition to the standard active power-frequency (P-ω) and reactive power-voltage (Q-V) droop controllers, as well as the inner voltage and current control loops. The VFI loop decouples the control of the active and reactive power, thus enhancing the sharing of reactive power. The VHI loop counteracts the effect of grid-side inductance by the negative inductance, and then the sharing of harmonic currents among all the DG inverters can be realized by adjusting the positive resistance. Moreover, in the presence of harmonic resonance, the VHI loop can shift harmonic resonant points toward a higher frequency range, in which the resonance can be more easily damped. Laboratory tests results are shown to validate the performance of the proposed control scheme.

II. Harmonic Current Filtering and Resonance Damping Approaches

This section reviews two autonomous control approaches for harmonic current filtering and resonance damping in an islanded microgrid. The effect of grid-side inductance on the performance of these methods is discussed.

A. System Configuration

Fig. 1 illustrates an example of a low-voltage microgrid dominated by multiple inverter-interfaced DG units. A static switch is used to dynamically disconnect the microgrid from the upstream distribution system during abnormal conditions. For the local and common loads, the diode rectifiers are used to denote the nonlinear loads, whereas the shunt capacitors represent the aggregated effect of capacitive loads and the capacitors in the *LCL*-filters of the grid-connected converters like battery chargers and active front-end rectifiers [4].

During the islanded operation, microgrid voltages usually becomes more sensitive to harmonic currents produced from the nonlinear loads, due to the limited power capacity of DG units and the low short-circuit ratio. Moreover, the presence of shunt capacitors tends to result in harmonic resonance and propagation throughout the microgrid. As a consequence, the mitigation of circulating harmonic current among all the DG units is needed to prevent overloading of some DG inverters, and meanwhile, proper resonance damping measures are also important to suppress harmonic voltage amplifications.

B. R-APF-Based Approach

Fig. 2 illustrates the block diagram of the R-APF-based control approach for the ith DG unit. The dc-link voltage of the DG inverter is regulated on the energy source side, and is assumed to be constant. The basic idea behind this method is to make the DG inverter operate as a resistor at the harmonic frequencies. It is realized by multiplying the output harmonic voltages of a DG inverter with a conductance, which is then passed through a high-bandwidth inner current controller [6]. The sharing of harmonic currents among all the DG inverters is achieved by adjusting the conductance through a harmonic var droop (H_i-G_i) controller [7].

Under this control scheme, Fig. 3 depicts the equivalent circuit of the islanded microgrid at the harmonic frequencies, where nonlinear loads are equivalent to the harmonic current

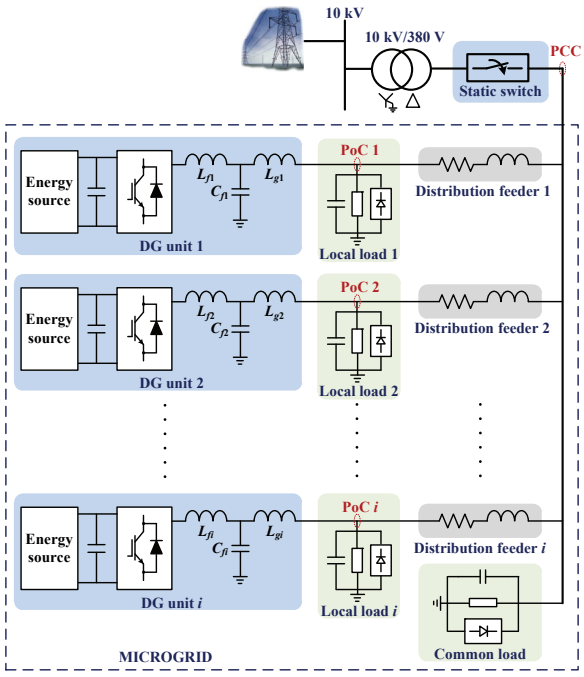

Fig. 1. A sample low-voltage microgrid dominated with multiple inverter-interfaced DG units.

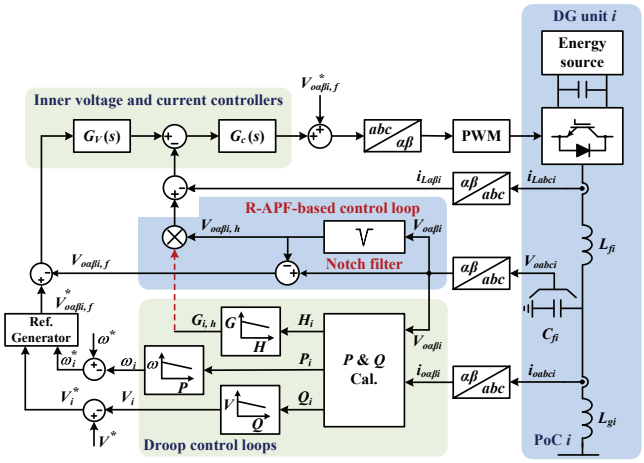

Fig. 2. Control block diagram of the Resistive-Active Power Filter (R-APF)-based approach.

sources for the sake of simplicity. Notice that different from the islanded network in [7], the sharing of harmonic currents not only depends on the designed conductance G_i, but also is affected by the size of the grid-side inductance. Furthermore, the grid-side inductance of the DG inverter also changes the characteristic impedance of a distribution feeder, which may result in an under-damped PoC voltage due to the 'whack-a-mole' effect [15]. Also, the large grid-inductance of the DG inverter tends to limit the bandwidth of the current controller.

C. Virtual Output Impedance Scheme

Fig. 4 illustrates the control block diagram of the virtual output impedance scheme [9]-[12]. This approach essentially builds a frequency-dependent droop relationship between the

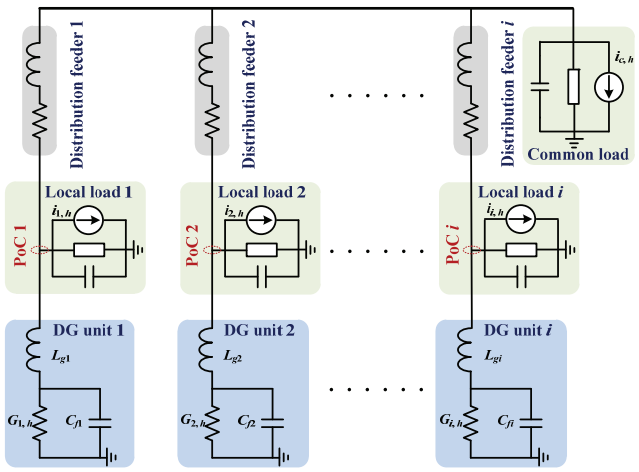

Fig. 3. Equivalent circuit of the islanded microgrid with the R-APF-based approach at the harmonic frequencies.

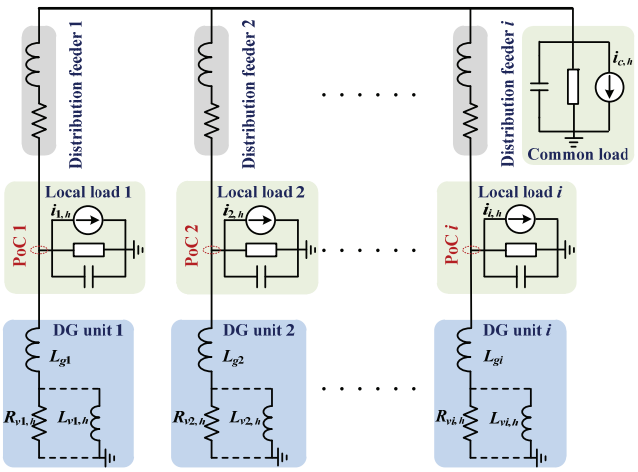

Fig. 5. Equivalent circuit of the islanded microgrid with the virtual output impedance scheme at the harmonic frequencies.

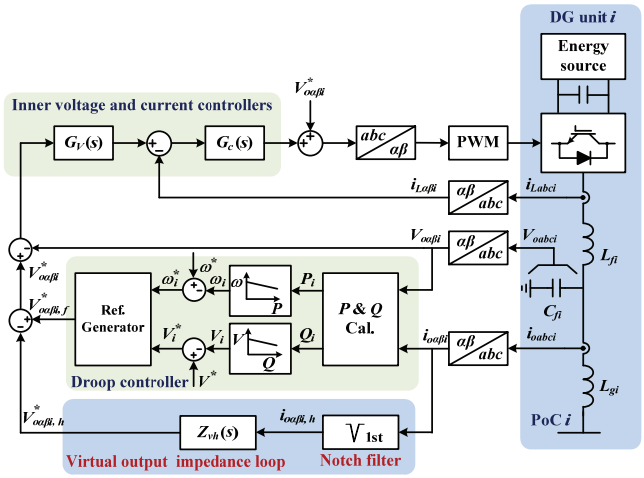

Fig. 4. Control block diagram of the virtual output impedance scheme.

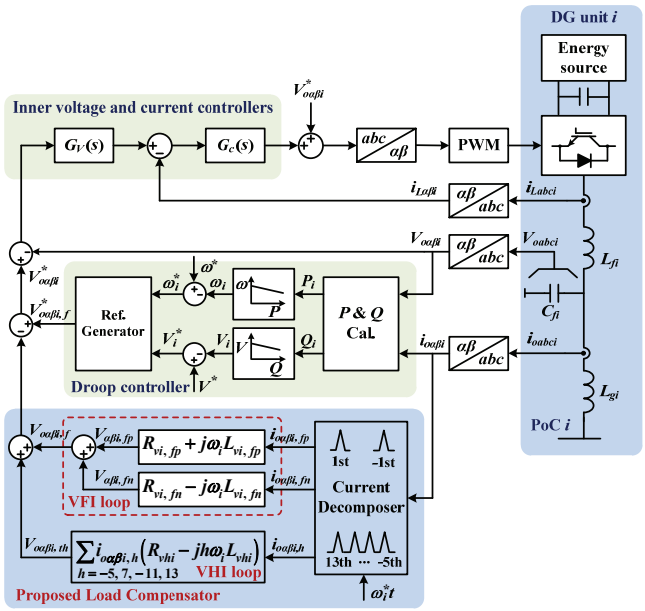

Fig. 6. Block diagram of the proposed control method using a load compensator

output harmonic voltage and the supplied harmonic current of a DG inverter by using a load current feedforward loop. A notch filter at the fundamental-frequency is used to detect the harmonic currents. Either the virtual resistance or the virtual inductance can be synthesized in the feedforward loop. Thus, the sharing of harmonic currents among all the DG inverters can be ensured at the expense of the additional harmonic voltages. As a consequence, a trade-off has to be considered when designing the virtual output impedance.

With the virtual output impedance loop, Fig. 5 shows the equivalent circuit of the islanded microgrid at the harmonic frequencies. Similarly, the nonlinear loads are simplified as harmonic current sources. The DG inverters are equivalent as either resistances or inductances, where the output capacitors are absent because of the high-bandwidth voltage controllers. Notice that the virtual resistances are more attractive than the virtual inductances, particularly on the damping of harmonic resonance. Nevertheless, large grid-side inductances usually require larger virtual resistances to take effect, which on the other hand lead to more severe harmonic voltage distortions.

III. Proposed Control Method

Fig. 6 shows the block diagram of the proposed control method of the *i*th DG unit, which comprises the inner voltage and current control loops, the *P*-ω and *Q*-*V* droop controller, as well as the load compensator including the VFI and VHI loops. Compared to the conventional virtual impedance loop, the VHI loop synthesizes the positive resistance and negative inductance at the dominant harmonic frequencies, such that the adverse effect of large grid-side inductance can be significantly counteracted [14]. The VFI loop is split into two impedances for the positive- and negative-sequence load currents, respectively. The positive-sequence VFI is mainly used to facilitate the use of *Q*-*V* droop for sharing reactive power, whereas the negative-sequence VFI is adopted to attenuate the negative-sequence circulating current [16].

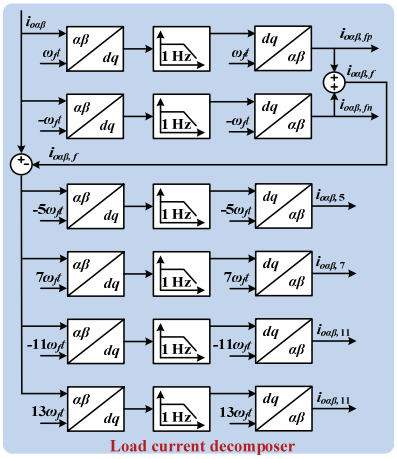

Fig. 7. Block diagram of the MSRFs-based load current decomposer.

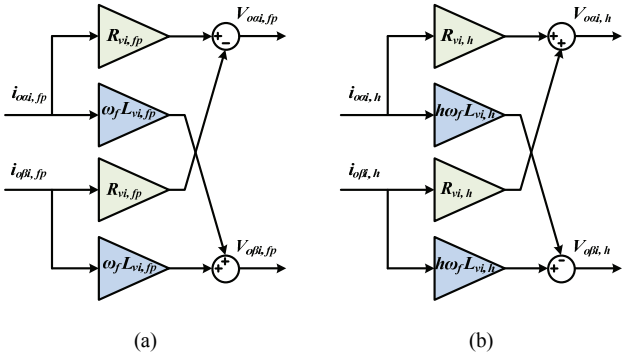

Fig. 8. Diagrams of the building blocks used for realizing (a) the Virtual Fundamental-Frequency positive-sequence Impedance, and (b) the Variable Harmonic Impedance.

A. Load Current Decomposer

From Fig. 6, it is seen that the decomposition of the load current i_{oabci} is important for realizing the load compensator. A number of power signal decomposition schemes have been developed recently, but the Multiple Synchronous Reference Frames (MSRFs) theory is still considered as one of the best solutions [17].

Fig. 7 shows the block diagram of the MSRFs-based load current decomposer, where the detection of the positive- and negative-sequence fundamental-frequency currents as well as the dominant harmonic currents is performed by a set of Park transformations and low-pass filters. Notice that the cut-off frequency of low-pass filters in the load current decomposer is designed with the same value as the low-pass filters for the calculation of active and reactive powers. Thus, the response of the VFI loop matches well with the dynamic of the droop-based power controller, and the slope of the *Q-V* droop can be dynamically adjusted. Furthermore, since the harmonics by definitions are steady-state distortions, the low-pass filters in the VHI loop can be chosen with low cut-off frequencies. Hence, low-pass filters with 1 Hz cut-off frequency are used in the load current decomposer.

B. Design of the VFI and VHI Loops

Fig. 8 shows the diagrams of the building blocks for the VFI and VHI loops, which can be derived as

$$\begin{pmatrix} V_{oai,\,fp} \\ V_{o\beta i,\,fp} \end{pmatrix} = \begin{pmatrix} R_{vi,\,fp} & -\omega_f L_{vi,\,fp} \\ \omega_f L_{vi,\,fp} & R_{vi,\,fp} \end{pmatrix} \begin{pmatrix} i_{oai,\,fp} \\ i_{o\beta i,\,fp} \end{pmatrix} \tag{1}$$

$$\begin{pmatrix} V_{oai,\,fn} \\ V_{o\beta i,\,fn} \end{pmatrix} = \begin{pmatrix} R_{vi,\,fn} & \omega_f L_{vi,\,fn} \\ -\omega_f L_{vi,\,fn} & R_{vi,\,fn} \end{pmatrix} \begin{pmatrix} i_{oai,\,fn} \\ i_{o\beta i,\,fn} \end{pmatrix} \tag{2}$$

$$\begin{pmatrix} V_{oai,\,h} \\ V_{o\beta i,\,h} \end{pmatrix} = \begin{pmatrix} R_{vi,\,h} & h\omega_f L_{vi,\,h} \\ -h\omega_f L_{vi,\,h} & R_{vi,\,h} \end{pmatrix} \begin{pmatrix} i_{oai,\,h} \\ i_{o\beta i,\,h} \end{pmatrix} \tag{3}$$

where the '*fp*' and '*fn*' represent the fundamental-frequency positive- and negative-sequence components, and '*h*' denotes the dominant harmonic components which can be -5, 7, -11, and 13. ω_f is the system fundamental-frequency. Notice that the diagram of the negative-sequence VFI is omitted, since it is conjugated to the positive-sequence VFI in Fig. 8 (a).

It is well known that the high R/X impedance ratio of the distribution feeders affects the performance of the *Q-V* droop for sharing reactive power [18]. To mitigate such effect, the positive-sequence VFI is designed only with an inductance. In contrast, the negative-sequence VFI is formed by a large resistance in the absence of unbalanced load [16].

The design of negative inductances in the VHI loop has been addressed in [14], where a 30% to 80% of the grid-side inductance is typically chosen, considering 20% variation of circuit constants in practical applications. Fig. 9 depicts the equivalent circuit of the islanded microgrid with VHI loop at the dominant harmonic frequencies. In contrast to Fig. 5, the harmonic inductances at the PoC of DG units are reduced by using the VHI loop. Hence, the harmonic impedances seen from the PoC of the DG unit are dominated by the positive resistances. Then, a good compromise between the sharing of harmonic currents and the resonance damping ability is needed when designing the resistances in the VHI loop.

C. Output Impedance Analysis

It is noted that the dynamic behaviors of the inner voltage and current control loops affect the output impedance profile of a DG inverter, which can be expressed as follows

$$V_o(s) = G_{cl}(s)V_o^*(s) - Z_o(s)I_o(s) \tag{4}$$

$$G_{cl}(s) = \left.\frac{V_o(s)}{V_o^*(s)}\right|_{I_o(s)=0} = \frac{G_c(s)G_d(s)G_V(s)}{L_f C_f s^2 + \left(G_c(s)G_d(s)+r_f\right)C_f s + G_c(s)G_d(s)G_V(s)} \tag{5}$$

$$Z_o(s) = \left.\frac{V_o(s)}{I_o(s)}\right|_{V_o^*(s)=0} = \frac{L_f s + r_f + G_c(s)G_d(s)}{L_f C_f s^2 + \left(G_c(s)G_d(s)+r_f\right)C_f s + G_c(s)G_d(s)G_V(s)} \tag{6}$$

where $V_o(s)$ and $V_o^*(s)$ are the actual and referenced inverter

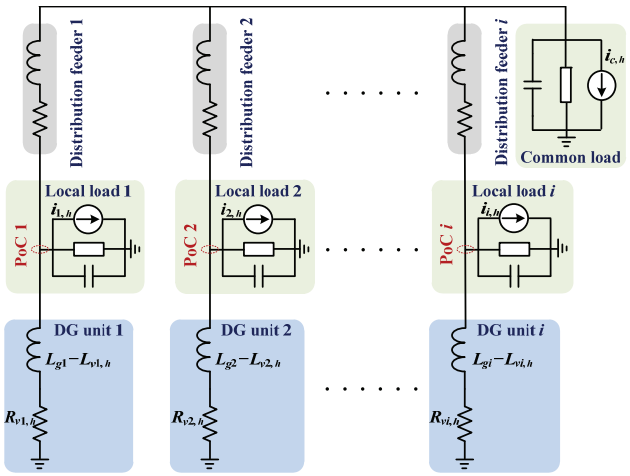

Fig. 9. Equivalent circuit of the islanded microgrid with the VHI loop at the dominant harmonic frequencies.

output voltages, respectively, $G_{cl}(s)$ denotes the closed-loop transfer function of the voltage control loops, and $Z_o(s)$ is the output impedance. r_f is the parasitic resistance of the filter inductance L_f. $G_d(s)$ is the 1.5 sampling period (T_s) delay, which includes the computational delay (T_s) and the PWM delay ($0.5T_s$) [19]. $G_c(s)$ is the proportional inductor current controller, and $G_V(s)$ denotes the capacitor voltage controller with a proportional and multiple resonant integral terms.

$$G_d(s) = \frac{1}{1+1.5T_s s} \tag{7}$$

$$G_V(s) = K_{pv} + \frac{K_{ivf}s}{s^2+\omega_f{}^2} + \sum_{\substack{h=-5,7,\\-11,13}} \frac{K_{ivh}s}{s^2+(h\omega_f)^2} \tag{8}$$

Considering the effect of the load compensator, the total output impedance $Z_{to}(s)$ can be derived by

$$Z_{to}(s) = G_{cl}(s)\left(Z_{v,fp}(s) + Z_{v,h}(s)\right) + Z_o(s) \tag{9}$$

$$Z_{v,fp}(s) = \frac{-2\omega_c(\omega_f)^2 L_{v,fp}}{s^2+2\omega_c s+(\omega_f)^2} \tag{10}$$

$$Z_{v,h}(s) = \sum_{h=5,7,11,13} \frac{2\omega_c(R_{v,h}s-(h\omega_f)^2 L_{v,h})}{s^2+2\omega_c s+(h\omega_f)^2} \tag{11}$$

where $Z_{v,fp}(s)$ is the positive-sequence VFI and $Z_{v,h}(s)$ is the VHI. Notice that the MSRFs-based load current decomposer can be transformed into the stationary frame by [20]

$$H_{BPF}(s) = H_{LPF}\left(\frac{s^2+(h\omega_f)^2}{2s}\right) = \frac{2\omega_c s}{s^2+2\omega_c s+(h\omega_f)^2} \tag{12}$$

where ω_c is the cut-off frequency of low-pass filters in Fig. 7, 2π rad/s. The effect of negative-sequence VFI is omitted, since it is only for attenuating circulating current.

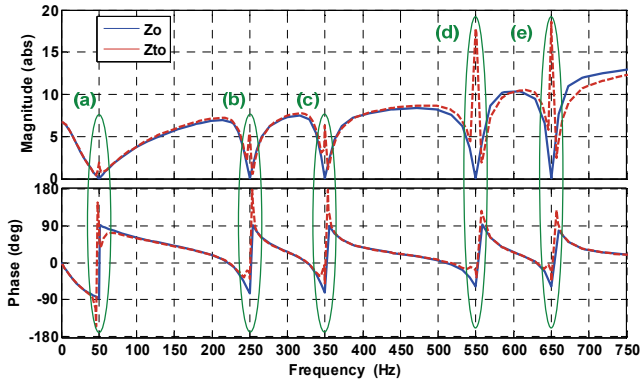

Fig. 10. Comparison between the characteristics of the output impedance $Z_o(s)$ and the total output impedance $Z_{to}(s)$.

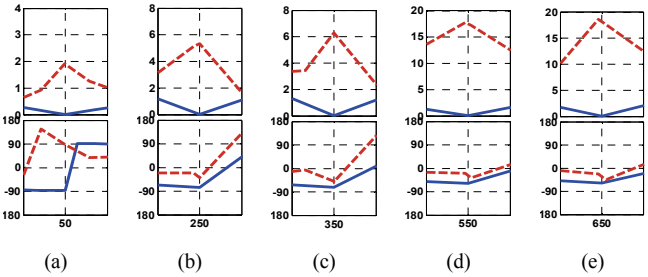

Fig. 11. Expanded view of Fig. 10.

Fig. 10 gives a comparison between the characteristics of the output impedance $Z_o(s)$ and the total output impedance $Z_{to}(s)$. The parameters of the inverter and designed controller are given in Appendix A. An expanded view of Fig. 10 at both the fundamental and the dominant harmonic frequencies is given in Fig. 11. It is seen that the total output impedance is reshaped by the load compensator, where the fundamental-frequency inductance and the selective harmonic impedances with negative phase angles are synthesized.

IV. Laboratory Test Results

To confirm the performance of the proposed approach, a three-phase microgrid is built in the laboratory. Fig. 12 shows a simplified one-line diagram of the built microgrid. Two 5.5 kVA Danfoss frequency inverters are adopted as the DG inverters, which are powered by two constant dc voltage sources, respectively. The control algorithm is applied in the DS1006 dSPACE system with 10.5 kHz sampling frequency and a half-period interrupt shift. The controller parameters and microgrid circuit constants are shown in Appendix A.

Fig. 13 shows the measured bus voltage waveforms and the associated harmonic spectra without using any harmonic current filtering and harmonic resonance damping schemes. The harmonic spectra are based on the linear RMS values of the phase-A voltages. It can be seen that the fifth harmonic resonance appears in the laboratory test. Notice that in this case the multiple harmonic resonant integrators in the inner voltage control loops of the DG inverters are kept zero in order not to increase the circulating harmonic current, while the VFI loop is activated to minimize the negative-sequence

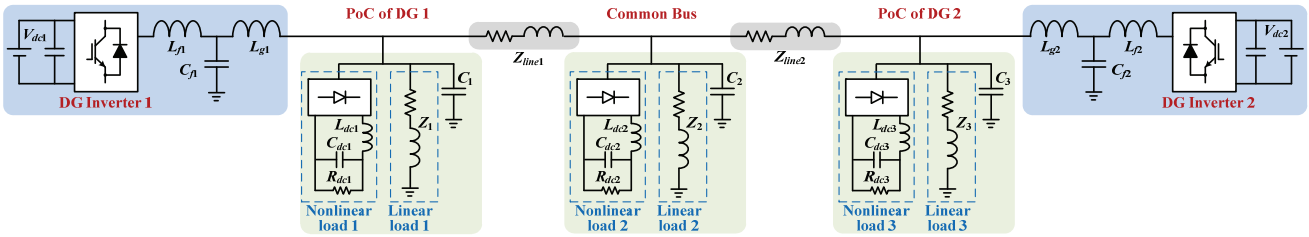

Fig. 12. Simplified one-line diagram of the built three-phase microgrid in laboratory.

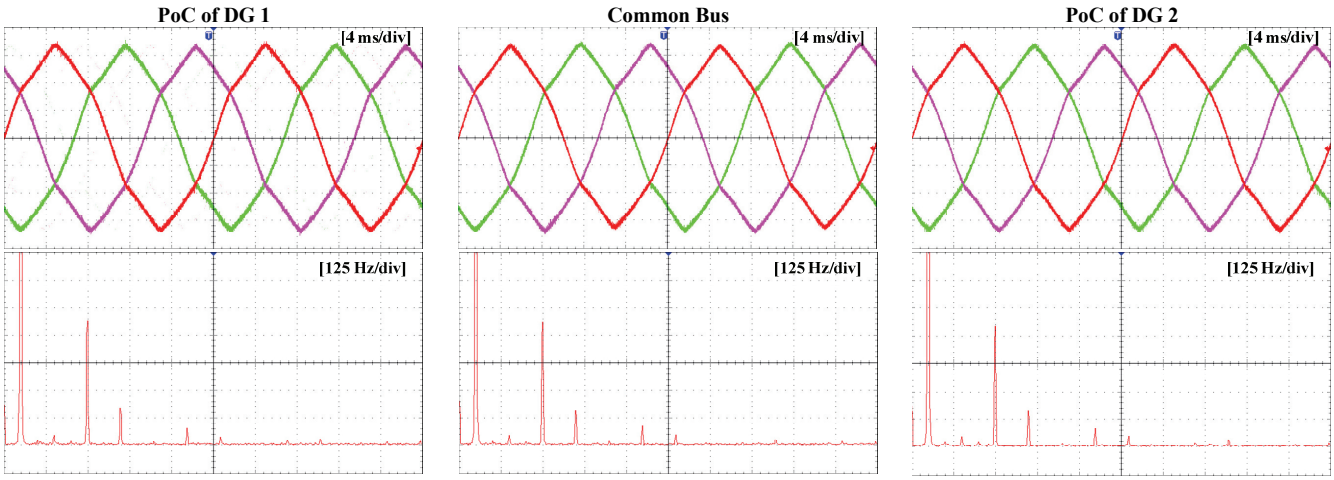

Fig. 13. Measured bus voltage waveforms (100 V/div) and the associated harmonic spectra (2 V_{RMS}/div) without using harmonic current sharing and resonance damping approach.

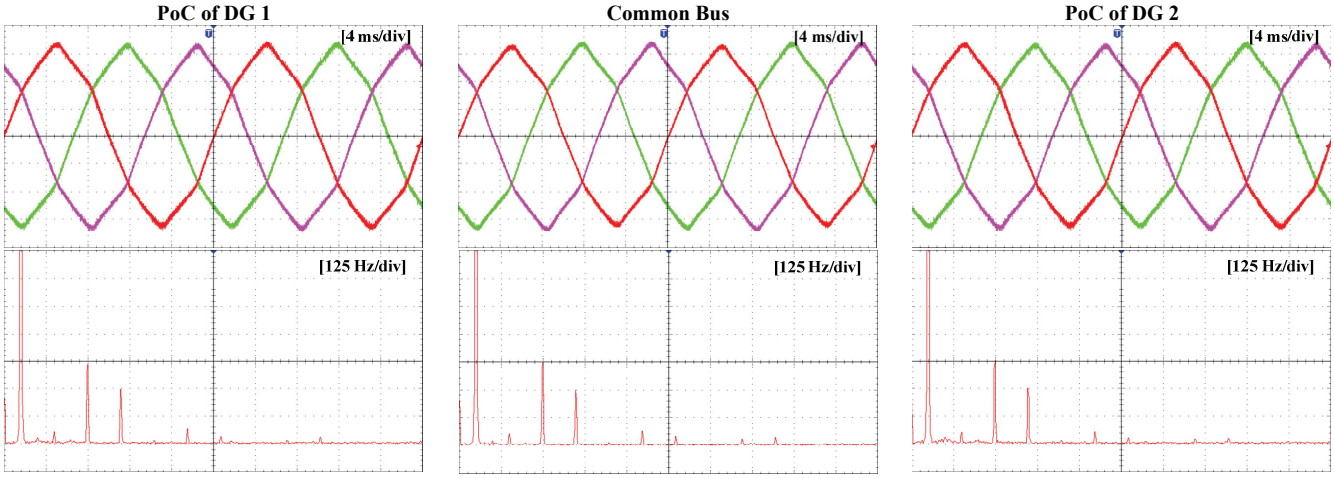

Fig. 14. Measured bus voltage waveforms (100 V/div) and the associated harmonic spectra (2 V_{RMS}/div) with the conventional virtual resistance scheme.

circulating current and reactive power difference. Fig. 16 (a) shows the output current waveforms of two inverters and the difference between them in this case. It is observed that the current difference is small due to the presence of large grid-side inductance.

Fig. 14 shows the measured bus voltage waveforms and the associated harmonic spectra with the conventional virtual resistance scheme [10]. In this case, only positive harmonic resistances in the VHI loop are activated. From the harmonic spectra, it is seen that the fifth harmonic voltages are reduced compared to Fig. 13, whereas the seventh harmonic voltages are increased. This indicates the presence of large grid-side inductances may bring a mismatch between the synthesized harmonic resistance and the characteristic impedance of the distribution feeder [15].

Furthermore, from Fig. 16 (b), it can be observed that the

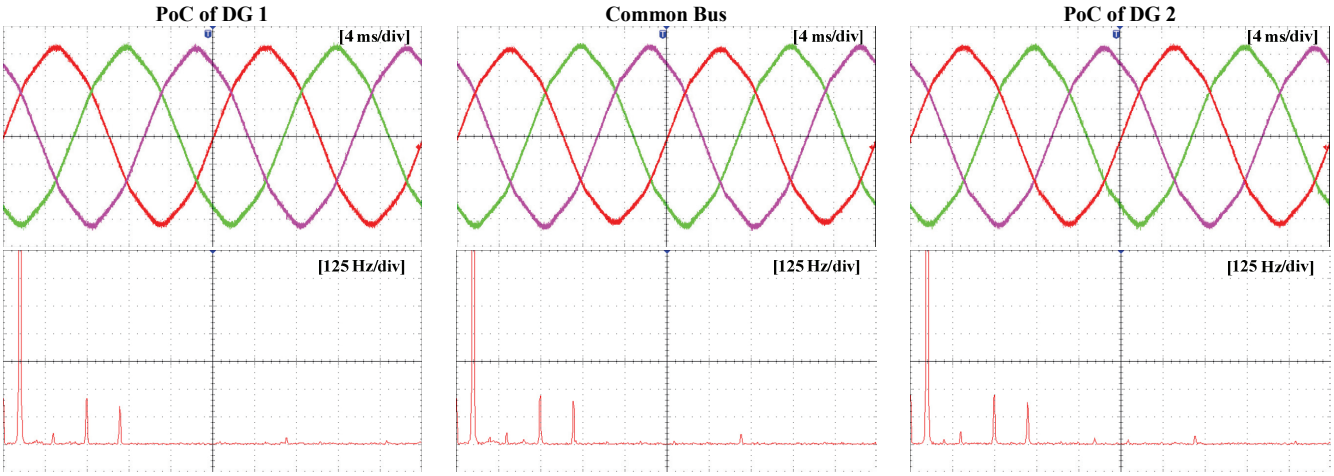

Fig. 13. Measured bus voltage waveforms (100 V/div) and the associated harmonic spectra (2 V_{RMS}/div) with the proposed control method.

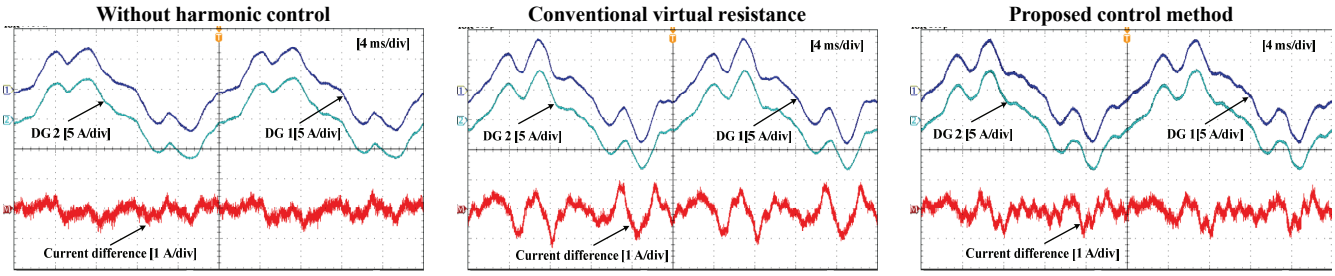

Fig. 14. Measured output current (Phase-A) waveforms of two DG inverters and the difference between them. (a) Without using harmonic current sharing and resonance damping approach. (b) With the conventional virtual resistance approach. (c) With the proposed control method.

output currents of the two inverters become more distorted due to the improvements of the bus voltages. Nevertheless, instead of mitigating the circulating harmonic currents as usual, it can be seen that the output current difference is even increased, which is because the phase angles of equivalent harmonic impedances of two inverters are different.

Fig. 15 shows the measured bus voltage waveforms and the associated harmonic spectra with the proposed control method. Compared to Fig. 13 and Fig. 15, it is obvious that the bus voltage waveforms become more sinusoidal. Also, as shown in the harmonic spectra, the fifth harmonic voltages are further damped without increasing the seventh harmonic voltages, which verifies the superior performance of the VHI loop than conventional virtual resistance loop. Table I shows the bus voltage Total Harmonic Distortions (THDs) for the three cases. Fig. 16 (c) shows the measured output current waveforms using the proposed control method. It is seen that the output currents become more severely distorted, but the current difference is reduced in comparison to Fig. 16 (b). It implies the designed load compensator can achieve harmonic current filtering and resonance damping autonomously.

Fig. 17 shows the measured transient waveforms of two inverters when the nonlinear loads at the PoC of DG 1 and the common bus are switched on. It is seen that the current difference first increases after switching on nonlinear loads, and then drops down to steady-state value. Although the bus voltages become distorted when the nonlinear loads increase, the harmonic resonance is still effectively damped.

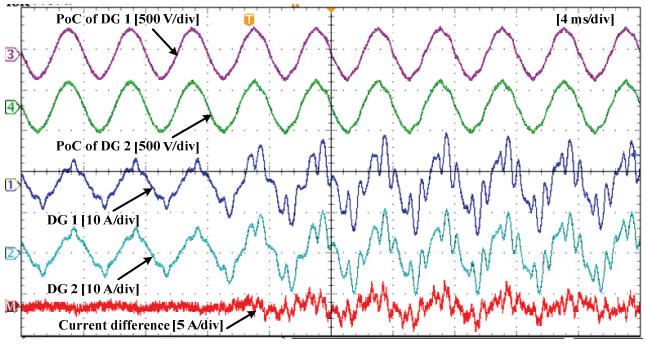

Fig. 17. Measured transient waveforms of two inverters when the nonlinear loads at the PoC of DG 1 and common bus are switched on.

TABLE I. BUS VOLTAGE THDS WITH DIFFERENT CONTROLLERS

Test Case	Voltage THD (%)		
	PoC of DG 1	*Common Bus*	*PoC of DG* 2
Without harmonic control (Fig. 13)	5.2	5.4	5.3
Conventional virtual resistance (Fig. 14)	4.1	4.4	4.2
Proposed control method (Fig. 15)	2.9	3.3	3.1

V. CONCLUSIONS

This paper has discussed harmonic current filtering and resonance damping methods of inverter-interfaced DG units in an islanded microgrid. Firstly, the block diagrams of the R-APF-based approach and the conventional virtual output impedance schemes were presented. The adverse effects of a large grid-side inductance on these two methods have been pointed out. Then, to overcome the problems in the presence of large grid-side inductances, a load compensator including a VFI loop and a VHI loop was proposed. It has been shown that the negative inductances in the VHI loop can effectively counteract the harmonic voltage drops across the grid-side inductance, while the positive harmonic resistances achieve harmonic current filtering and resonance damping. Finally, the laboratory tests of an islanded three-phase microgrid are performed to validate the theoretical analysis and expected performance of the proposed control method.

APPENDIX A

A. Power Stage Parameters of DG Inverters

- Switching frequency: 10 kHz
- DC link voltage: $V_{dc1} = V_{dc2} = 780$ V
- AC filter inductor: $L_{f1} = L_{f2} = 1.5$ mH
- AC filter capacitor: $C_{f1} = C_{f2} = 25$ μF
- Grid-side inductor: $L_{g1} = 2$ mH, $L_{g2} = 3$ mH

B. Microgrid Circuit Constants

- System fundamental-frequency: 50 Hz
- Nominal voltage: 380 V
- Distribution feeders: $R_{line1} = R_{line2} = 0.2\ \Omega$
  $L_{line1} = L_{line2} = 0.25$ mH
- Shunt capacitors: $C_1 = C_2 = C_3 = 50$ μF
- Linear loads: $Z_1 = Z_3 = 4.3$ kVA, PF = 0.3
  $Z_2 = 0.3$ kW
- Nonlinear loads: $L_{dc1} = L_{dc2} = L_{dc3} = 84$ μH
  $C_{dc1} = C_{dc2} = C_{dc3} = 235$ μF
  $R_{dc1} = 0.9$ kW, $R_{dc2} = R_{dc3} = 0.6$ kW

C. Proposed Controller Parameters

- Sampling frequency: 10.5 kHz
- Current controller: $K_{pc1} = K_{pc2} = 10$
- Voltage controller: $K_{pv1} = K_{pv2} = 0.15$
  $K_{ivf1} = K_{ivf2} = 120$
  $K_{iv5,1} = K_{iv7,1} = K_{iv11,1} = K_{iv13,1} = 30$
  $K_{iv5,2} = K_{iv7,2} = K_{iv11,2} = K_{iv13,2} = 30$
- Droop controller: $n_{p1} = n_{p2} = 10^{-4}$, $m_{p1} = m_{p2} = 10^{-3}$
- VFI loop: $L_{vfp1} = L_{vfp2} = 6$ mH
  $R_{vfn1} = R_{vfn2} = 20\ \Omega$
- VHI loop: $L_{v5,1} = L_{v7,1} = L_{v11,1} = L_{v13,1} = 1.5$ mH
  $R_{v5,1} = R_{v7,1} = 4\ \Omega$, $R_{v11,1} = R_{v13,1} = 16\ \Omega$
  $L_{v5,2} = L_{v7,2} = L_{v11,2} = L_{v13,2} = 2.25$ mH
  $R_{v5,2} = R_{v7,2} = 4\ \Omega$, $R_{v11,2} = R_{v13,2} = 16\ \Omega$

REFERENCES

[1] R. Lasseter, "Smart distribution: Coupled microgrids," IEEE Proc., vol. 99, no. 6, pp. 1074-1082, Jun. 2011.

[2] X. Wang, J. M. Guerrero, F. Blaabjerg, and Z. Chen, "A review of power electronics based microgrids," *Journal of Power Electron.*, vol. 12, no. 1, pp. 181-192, Jan. 2012.

[3] X. Wang, J. M. Guerrero, F. Blaabjerg, and Z. Chen, "Secondary voltage control for harmonic suppression in islanded microgrids," *in Proc. IEEE PESGM* 2011, pp. 1-8.

[4] J. H. Enslin and P. J. Heskes, "Harmonic interaction between a large number of distributed power inverters and the distribution network," *IEEE Trans. Power Electron.,* vol. 19, no. 6, pp. 1586-1593, Nov. 2004.

[5] F. Wang, J. Duarte, M. Hendrix, and P. Ribeiro, "Modelling and analysis of grid harmonic distortion impact of aggregated DG inverters," *IEEE Trans. Power Electron.*, vol. 26, no. 3, pp. 786-797, Mar. 2011.

[6] T. Takeshita and N. Matsui, "Current waveform control of PWM converter system for harmonic suppression on distribution system," *IEEE Trans. Ind. Electron.*, vol. 50, no. 6, pp. 1134-1139, Dec. 2003.

[7] T. Lee, and P. T. Cheng, "Design of a new cooperative harmonic filtering strategy for distributed generation interface converters in an islanding network," *IEEE Trans. Power Electron.*, vol. 22, no. 5, pp. 1919-1927, Sep., 2007.

[8] X. Wang, F. Blaabjerg, Z. Chen, and J. M. Guerrero, "A centralized control architecture for harmonic voltage suppression in islanded microgrids," in *Proc. IEEE IECON* 2011, pp. 3070-3075.

[9] U. Borup, F. Blaabjerg, and P. Enjeti, "Sharing of nonlinear load in parallel-connected three-phase converters," *IEEE Trans. Ind. Appl.*, vol. 37, no. 6, pp. 1817-1823, Nov./Dec., 2001.

[10] D. De and V. Ramanarayanan, "Decentralized parallel operation of inverters sharing unbalanced and non-linear loads," *IEEE Trans. Power Electron.*, vol. 25, no. 12, pp. 1126-1132, Dec. 2010.

[11] T. Vandoorn, B. Meersman, J. D. Kooning, and L. Vandevelde, "Controllable harmonic current sharing in islanded microgrids: DG units with programmable resistive behavior toward harmonics," *IEEE Trans. Power Del.*, vol. 27, no. 2, pp. 831-841, Apr. 2012.

[12] S. J. Chiang and J. M. Chang, "Parallel control of the ups inverters with frequency-dependent droop scheme," in *Proc. IEEE PESC* 2001, pp. 957-961.

[13] J. He, Y. W. Li, and M. S. Munir, "A flexible harmonic control approach through voltage-controlled DG-grid interfacing converters," *IEEE Trans. Ind. Electron.*, vol. 59, no. 1, pp. 444-455, Jan. 2012.

[14] X. Wang, F. Blaabjerg, and Z. Chen, "Synthesis of variable harmonic impedance in inverter-interfaced distributed generation unit for harmonic resonance damping throughout a distribution network," *IEEE Trans. Ind. Appl.*, in press, 2012.

[15] K. Wada, H. Fujita, and H. Akagi, "Considerations of a shunt active fitler based on voltage detection for installation on a long distribution feeder," *IEEE Trans. Ind. Appl.*, vol. 38, no. 4, pp. 1123-1130, Jul./Aug. 2002.

[16] X. Wang, F. Blaabjerg, and Z. Chen, "An improved virtual impedance for droop-controlled parallel three-phase voltage source inverters," in *Proc. IEEE ECCE* 2012, in press, 2012.

[17] V. Moreno, M. Liserre, A. Pigazo, and A. Dell'Aquila, "A comparative analysis of real-time algorithms for power signal decomposition in multiple reference frames," *IEEE Trans. Power Electron.*, vol. 22, no. 4, pp. 1280-1289, Jul. 2007.

[18] J. He and Y. W. Li, "Analysis, design, and implementation of virtual impedance for power electronics interfaced distributed generation," *IEEE Trans. Ind. Appl.*, vol. 47, no. 6, pp. 2525-2538, Nov./Dec. 2011.

[19] V. Blasko and V. Kaura, "A new mathematical model and control of a three-phase AC-DC voltage source converter," *IEEE Trans. Power Electron.*, vol. 12, no. 1, pp. 116-123, Jan., 1997.

[20] D. N. Zmood and D. G. Holmes, "Stationary frame current regulation of PWM inverters with zero steady-state error," *IEEE Trans. Power Electron.*, vol. 18, no. 3, pp. 814-822, May, 2003.